JACS
JOURNAL OF THE AMERICAN CHEMICAL SOCIETY

Article

pubs.acs.org/JACS

Simultaneous Growths of Gold Colloidal Crystals

Nicolas Goubet,[†] Hervé Portalès,[†] Cong Yan,[†] Imad Arfaoui,[†] Pierre-Antoine Albouy,[‡] Alain Mermet,[§] and Marie-Paule Pileni*,[†]

[†]Université Pierre et Marie Curie and Centre National de la Recherche Scientifique, UMR 7070, LM2N, 4 Place Jussieu, 75005 Paris, France

[‡]Laboratoire de Physique des Solides, Université Paris-Sud, UMR 8502, 91405 Orsay, France

[§]Laboratoire de Physico-Chimie des Matériaux Luminescents, Université Lyon1, UMR 5620, Centre National de la Recherche Scientifique, Bât. A. Kastler, 10 rue Ada Byron, 69622 Villeurbanne, France

Supporting Information

ABSTRACT: Natural systems give the route to design periodic arrangements with mesoscopic architecture using individual nanocrystals as building blocks forming colloidal crystals or *supracrystals*. The collective properties of such supracrystals are one of the main driving forces in materials research for the 21st century with potential applications in electronics or biomedical environments. Here we describe two simultaneous supracrystal growth processes from gold nanocrystal suspension, taking place in solution and at the air−liquid interface. Furthermore, the growth processes involve the crystallinity selection of nanocrystals and induce marked changes in the supracrystal mechanical properties.

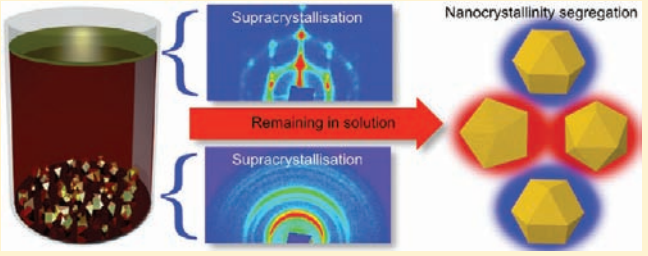

1. INTRODUCTION

About five billion years ago in the early solar system, highly uniform magnetite particles of few hundred nanometers in size were assembled in three-dimensional (3D) arrays.[1] Thirty million years ago, silicate particles with submicrometer size were self-organized in the form of opal.[2] Opal is colorless when composed of disordered silicate particles, whereas it shows specific reflectivity when particles are organized in arrays. This change in the optical properties reveals the emergence of intrinsic properties when particles are ordered on large scale. Nowadays, in the era of nano, it is found that nanocrystals (NCs) can self-assemble in crystallographic orders called supracrystals. Such suprastructures, which enable the design of novel materials, are expected to become one of the main driving forces in material research for the 21st century.[3,4] However, mimicking the natural processes at nanoscale remains a challenge. Over the past decade, many reports have revealed the intrinsic chemical and physical properties induced by the two-dimensional (2D) ordering of NCs,[5−10] while the characteristics of 3D supracrystals, such as the mechanical, vibrational, magnetic, and energy transfer properties, still suffer from a lack of knowledge.[11−15] These potential changes in the chemical and physical properties of supracrystals will open a new research area not only from the fundamental viewpoint but also for future applications.[16]

In the recent past, supracrystal elaboration was limited by the growth mechanism (either homogeneous or heterogeneous growth), which resulted in the formation of only one type of supracrystals.[17−24] Here, for the first time, we report the simultaneous growth of two types of Au supracrystals. The experiments were performed under toluene-saturated atmosphere in thermodynamic equilibrium. It was found that at the air−toluene interface, thick and layer-by-layer supracrystals are formed, whereas in solution a homogeneous growth takes place with precipitation of supracrystals randomly oriented and characterized either by three- and five-fold symmetries or polycrystal structures. The simultaneous growth processes favor selection of nanoparticle crystallinity, called nanocrystallinity, for small nanocrystal sizes. Furthermore, the mechanical properties of the interfacial and precipitated supracrystals markedly depend on nanocrystallinity and on the supracrystal growth mechanism.

2. EXPERIMENTAL SECTION

Nanocrystal Synthesis. The synthesis of gold NCs with various sizes (from 4 to 8 nm) has been reported in a previous paper.[17] In a typical synthesis, (PPh_3)Au−Cl molecular precursor is dissolved in toluene under nitrogen protection. After the clear solution is heated at 100 °C, a certain amount of dodecanethiol is added under a vigorous stirring. A reductive solution is made of amine−borane complex dissolved in toluene and heated at the same temperature. When both solutions are stabilized, they are mixed together. The formation of gold NCs is revealed by a color change from colorless to bright brown to dark red. Changing the amount of dodecanethiol and reducing agent allows controlling the size of the NCs. The colloidal solution is washed by precipitation in ethanol. The NCs can be redispersed in toluene to self-assemble.

Experimental Setup. Conventional scanning electron microscopy (SEM) images were obtained from a JEOL JSM-5510LV, and the high

Received: August 29, 2011
Published: February 13, 2012

   dx.doi.org/10.1021/ja207941p | *J. Am. Chem. Soc.* 2012, 134, 3714−3719

resolution images SEM were recorded from a Hitachi SU-70. The conical dark-field measurements were carried out using a JEOL JEM 2010 at 200 kV, and the tilted electron beam makes a motion of precession at 1.6 Hz.

Grazing incidence small-angle X-ray diffraction (GISAXRD) experiments are performed with a rotating copper anode generator operated with a small-size focus (0.1 × 0.1 mm^2 in cross-section) at 40 kV and 20 mA. The optics consists of two parabolic multilayer-graded mirrors in K-B geometry. It delivers a well-defined and intense parallel monochromatic beam. A photostimulable phosphor plate is used as detector. The reading of the exposed imaging plate is performed by a scanner (STORM 820 Molecular Dynamics).

Low-frequency Raman scattering (LFRS) spectra are recorded in a classical backscattering geometry with a six-pass tandem Fabry–Pérot interferometer. Monochromatic light emitted at 532 nm by a continuous yttrium aluminum garnet (YAG) laser is used as the excitation source.

The mechanical properties of the supracrystals are investigated using nanoindentation measurements with an atomic force microscopy (AFM) tip indenting into the material and pulling back to measure the elastic modulus. AFM experiments were performed using a commercial AFM 5100 System (Agilent Technologies, U.S.A.) using acoustic/contact mode AFM scanner interfaced with a PicoScan controller. Standard silicon AFM tips with spring constants of 4.5 N/m from MikroMasch were used for imaging and measuring the samples. Figure S1 is an illustration of the original data plot obtained from the nanoindentation measurements. An indentation analysis software called *Punias* was used for extracting the force versus penetration curve. This curve is used to deduce the Young's modulus. Each Young's modulus values are obtained for more than 10 measurements, and the median value is given in the paper. The AFM indentation is performed with the constant indentation depth (about 80 nm) regardless the NC sizes. For the nanoindentation measurements, a thermal K card is used to deduce the proper stiffness of the cantilever. For the contact area (i) first we took into account the manufacture's specifications of the tip. (ii) Second, we checked the shape of the AFM probe by SEM. (iii) Finally, the value of the contact area was verified by measuring the Young's modulus of a reference sample as Teflon foil.

3. RESULTS AND DISCUSSION

Simultaneous Growths of Supracrystals. Dodecanethiol-coated Au NCs with sizes varying from 4 to 8 nm and 6% size distribution are dispersed in toluene. NCs with average diameters of 4, 5, 6, 7, and 8 nm are employed in the present investigation. These NCs are referred to as Au_4, Au_5, Au_6, Au_7, and Au_8, respectively. The NCs consist of a mixture of monodomain NCs, multiply twinned particles (MTPs) with decahedral and icosahedral shapes and polycrystals. These features will be referred to as nanocrystallinity.

These NCs dispersed in toluene ($[Au] = 10^{-2}$ M) are kept in a beaker under a saturated toluene atmosphere. After 7 days, flocculation of NCs occurred at the air–toluene interface, resulting in a bright and thin interfacial film (Figure 1a). At the same time precipitates appear. As the aggregation of NCs in the form of film and precipitate continued, the Au NCs concentration in suspension decreases as revealed by the color of solution. Such a decrease is faster for larger NCs, indicating their ability to aggregate with a faster rate. The simultaneous formation of thin interfacial film and precipitate at the bottom is not seen in the beaker containing Au_4 NCs.

The interfacial film, withdrawn using a tungsten ring, is deposited on desired substrates. The precipitates are collected on highly oriented pyrolitic graphite (HOPG) for further analysis. The SEM images of Au_7 and Au_8 interfacial films are similar to those shown for Au_6 (Figure 1b). High-resolution SEM image shows (Figure 1c) a very large uniform orientation area indicating a long coherence length (>1 μm) with the presence of dislocations (see white arrows in Figure 1d). The crystalline structure of such assemblies is determined by GISAXRD. The patterns corresponding to the interfacial films remain similar for NCs at and above 6 nm. Various diffraction spots are observed and indexed by using an fcc lattice (Figure 1e). The average interparticle distance, δ, calculated from the d_{111} spacing is given in Table 1. For Au_5 interfacial films, the NC array (Figure 1f) is composed of coexisting domains with distorted three-fold and two-fold symmetries as supported by the Fourier transformed patterns of areas 1 and 2 (inset Figure 1f). The diffraction profile (Figure 1g) shows planes indexed as fcc and bcc structures. Irrespective of the NC sizes, the thickness of the interfacial supracrystal film is found to be in the range 200–300 nm. The interfacial supracrystal thickness could be tuned by varying the concentration of the mother suspension.

The precipitated supracrystals are collected, and SEM images show individual aggregates with well-defined shapes. Their sizes (1–10 μm) are larger with Au_5 (Figure 2a) than those obtained for larger NCs (Figure 2b). For any NC sizes, a powderlike pattern is obtained by GISAXRD (Figure 2c). The indexation of the *d*-spacings (Figure 2d) agrees with an fcc structure. The average interparticle distances, δ, for the precipitates (Table 1) are the same as for interfacial supracrystals.

Additionally three- and five-fold symmetries and various shapes are pointed out in Figure 2e–g as already observed in other experimental conditions.[25,26] Note the following: (i) for Au_5 NCs, the precipitated supracrystals are characterized by an fcc structure, whereas the interfacial supracrystals are a mixture of fcc/bcc structures; (ii) for any NC size, the precipitated supracrystals show that the 2D nucleation occurs on the surface of each facet (Figure 2h); (iii) dislocations observed on the interfacial film supracrystals (Figure 1d) do not exist in the corresponding precipitates (Figure 2h).

To explain the mechanism of these two simultaneous supracrystal growths we have to take into account on the one hand the attractive interactions between NCs and on the other hand the surface tension at the air/toluene interface. In a previous paper,[17] we demonstrated that, for large NC sizes (>5 nm), due to the solvent-mediated attraction between nanocrystals by the interparticle potential, supracrystals form within the solution by homogeneous nucleation. This clearly explains the growth of the precipitated supracrystals. Concerning the interfacial supracrystals, the trapping of NCs at the interface is governed by the attractive interaction potential between the NCs and the interface. This favors formation of the first close-packed monolayer. With increasing time, additional NCs from suspension are attracted by the first NC monolayer, thus inducing a progressive stacking of NC layers to reach formation of a well-defined supracrystal. Such an interfacial supracrystal growth mechanism is consistent with the fact that (i) the thickness of film decreases with diluting the colloidal mother suspension and (ii) the film thickness does not show any correlation with the NC size. It is found that for any NC sizes and growth mechanisms, the supracrystals are usually characterized by fcc structures, except with Au_5 interfacial film supracrystals which comprise a mixed fcc/bcc structure (Figure 1h). The mixed structure is explained by a recently developed model based on competitive effect between dense packing and minimization of contact surface between NCs.[27]

Specific Supracrystal Properties. These two kinds of supracrystals exhibit some unusual properties. The bright and

dx.doi.org/10.1021/ja207941p | J. Am. Chem. Soc. 2012, 134, 3714–3719

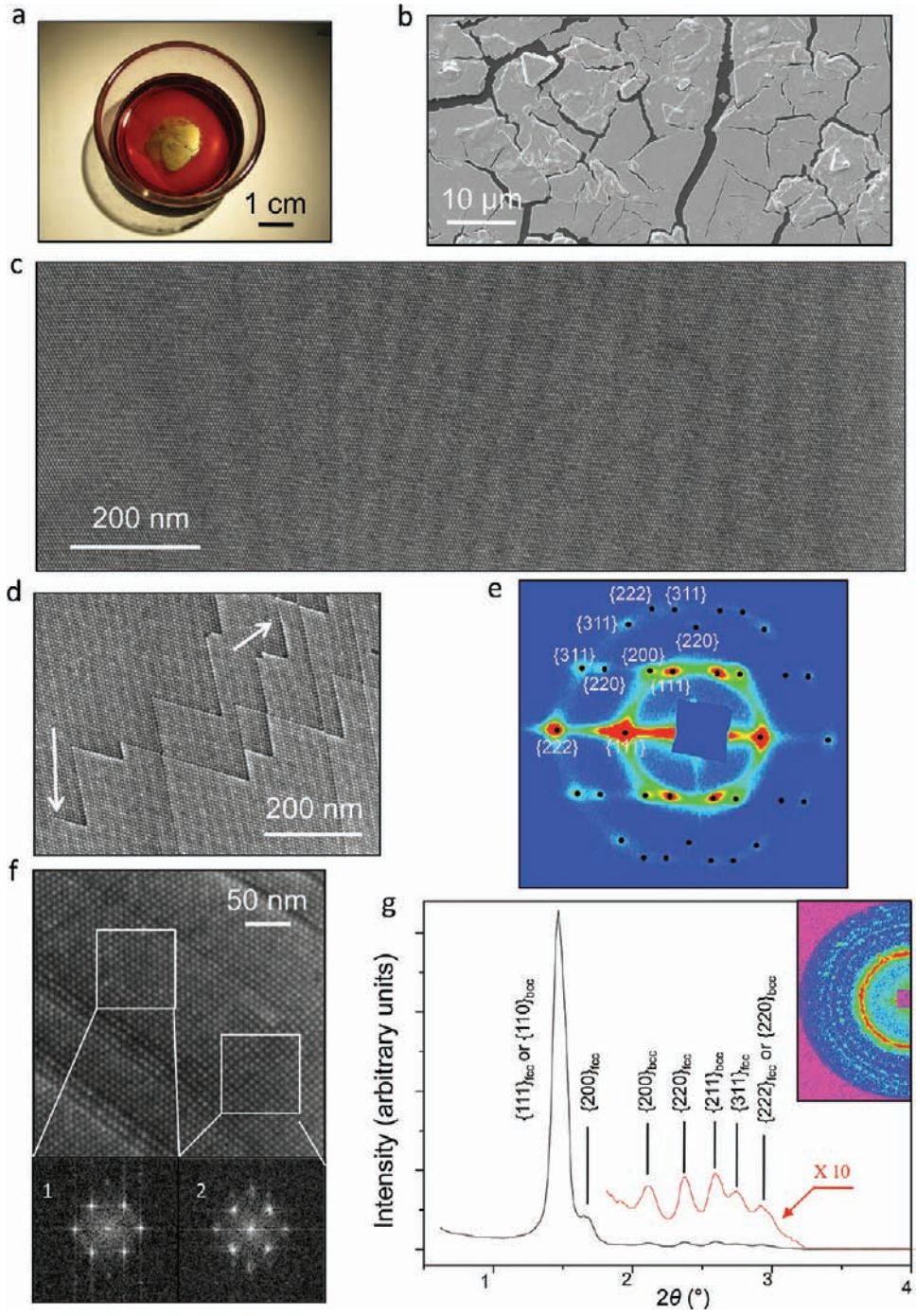

Figure 1. Upside view of the colloidal solution after 7 days (a). SEM image of the interfacial film (b). High-resolution SEM images of selected areas on the film showing a large domain (c) with sparse screw dislocations (d). Superimposed experimental and calculated (black points) GISAXRD pattern of interfacial film (e). The calculated one is based on an fcc-oriented powder along the [111] axis perpendicular to the substrate. High-resolution SEM image of Au_5 interfacial film (f) from distorted hexagonal (1) to distorted square (2) symmetry. One-dimensional (1D) and 2D (inset) SAXRD patterns acquired in transmission geometry (g).

conical dark-field TEM images (Figure 3a) obtained from the deposition of a drop of the colloidal solution show NCs with various contrasts. This difference corresponds to different nanocrystallinities.[28] Figure 3d displays monodomain NCs, characterized by a homogeneous contrast, whereas it is inhomogeneous for MTPs (Figure 3b) and polycrystals (Figure 3c).

The Au_5 interfacial film and precipitated supracrystals are extracted from the vessel and redispersed separately in hexane. A drop of suspension is deposited on the TEM grid. Panels e (interfacial) and g (precipitated) of Figure 3 show the resulting conic dark-field TEM images, characterized by a homogeneous contrast, indicating that the NCs are monodomain. By deposition of a drop of the solution in equilibrium with interfacial and precipitated supracrystals, the TEM image shows (Figure 3f) inhomogeneous contrast due to NCs characterized by either MTP or polycrystalline structures.

From these images, it is concluded that supracrystals (interfacial and precipitated) are composed of monodomain NCs,

dx.doi.org/10.1021/ja207941p | J. Am. Chem. Soc. 2012, 134, 3714–3719

Table 1. Nanocrystal Features and Evaluated Young's Modulus for Each Supracrystal

		Au_5	Au_6	Au_7	Au_8
mean diameter (nm)		5.2	6.1	7.0	7.8
diameter polydispersity (%)		7	6	6	8
interparticle distance (nm)	interface	2.3 ± 0.4	2.3 ± 0.4	2.1 ± 0.4	2.0 ± 0.3
	precipitate	2.1 ± 0.1	2.4 ± 0.4	2.6 ± 0.4	2.5 ± 0.3
Young's modulus (normalized)	interface	10.0	2.1	1.5	1
	precipitate	7.3	4.6	2.6	1
	precipitate/interface ratio	4.6	13.9	12.8	6.5

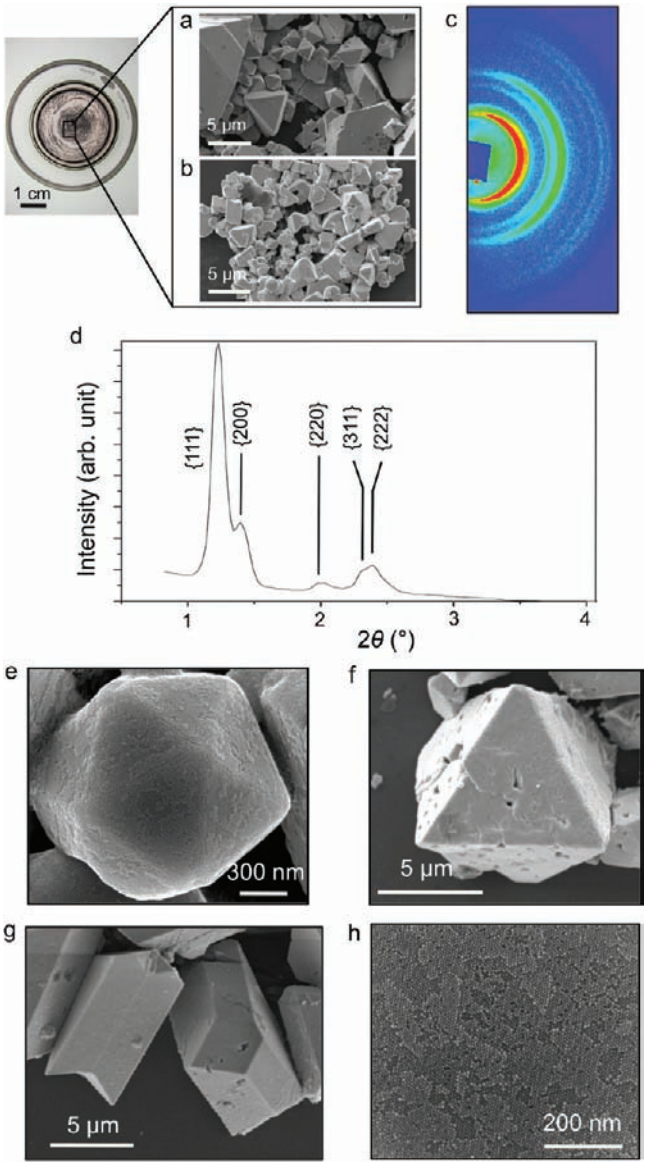

Figure 2. SEM image of the black powder for Au_5 (a) and Au_{6-8} (b). GISAXRD pattern of the precipitate (c,d). Five-fold symmetry shapes as icosahedron (e). Monocrystalline shape as octahedron (f). Association of two truncated tetrahedral single supracrystals on a spinel twin (g). High-resolution SEM image of a precipitated supracrystal surface (h).

whereas MTPs and polycrystals remain in solution. While the TEM images give local information, using low-frequency Raman scattering (LFRS) measurements enables obtaining reliable information on nanocrystallinity from larger population of NCs. As shown from a previous study of acoustic vibrations of Au NCs, this technique is indeed a valuable tool to distinguish between monodomain NCs and polycrystals.[28] In fact, a splitting of the quadrupolar modes in two-fold degenerate E_g modes and three-fold degenerate T_{2g} modes is observed for monodomain NCs. At variance, for MTPs and polycrystals only one band is observed due to light scattering by their quadrupolar vibrational modes.[28] The LFRS spectra (Figure 3h) of the Au_5 interfacial film as well as of the precipitated supracrystals exhibit two distinct Raman bands peaked around 135 and 210 GHz. In contrast, a multiple structured band with three components is observed in the spectrum of NCs remaining in suspension (Figure 3f). This multicomponent band is attributed to the mutual contributions of monodomain and polycrystalline NCs. This strongly confirms the selection of nanocrystallinity already observed by TEM. The presence of mainly monodomain NCs in supracrystals could be attributed to the fact that the {111} facets of monodomain NCs are larger than those of MTPs, thus favoring better attraction between NCs. From Figure S3, the observation of three component peaks in the Raman spectra of the Au_6 supracrystals indicates the presence of both MTPs and monodomain NCs. This decrease in the nanocrystallinity selection efficiency is more pronounced for the interfacial compared to the precipitated supracrystals and has to be related to the growth mechanisms

Figure 4a shows an acoustic mode AFM image of the surface of 3D Au_8 interfacial film deposited on HOPG. This morphology is consistent with the ordered structure seen in the SEM image (Figure 1c). To avoid any contribution of the substrate in the nanoindentation measurements, the interfacial supracrystal film is transferred onto a TEM grid that has 2.6 μm diameter circular holes with center-to-center distances of 4 μm (Figure S2). The AFM indentation (white arrows in Figure 4b) is then performed in the center of holes totally covered by the supracrystals without any cracks (Figure 4b). Similar measurements are also carried out with the precipitated ones. The Young's modulus, extracted from the uploading curve (Figure 4c), are in the GPa range, indicating a strong coupling between NCs consistent with measurements in contact mode (Figure 4d). Table 1 gives the ratios between interfacial and precipitated supracrystals for each nanoparticle size. The Young's modulus of the interfacial film is lower than that of the corresponding precipitated supracrystals. This is attributed to the change in the growth mechanisms of the superlattices. Note that the interfacial supracrystals show dislocations (Figure 1d), whereas these are absent in the precipitated ones (Figure 2h). This explains the decrease in the stiffness of the interfacial supracrystals as observed for bulk materials[29] where a drop of the Young's modulus is found due to the presence of dislocations. For any supracrystal growth, Table 1 shows a decrease of Young's modulus (normalized by the value of Au_8) with increasing the NC sizes, which is presumably related to the nanocrystallinity.

To support such claim we need to produce, by using the same growth mechanism, supracrystals formed by either single

dx.doi.org/10.1021/ja207941p | J. Am. Chem. Soc. 2012, 134, 3714–3719

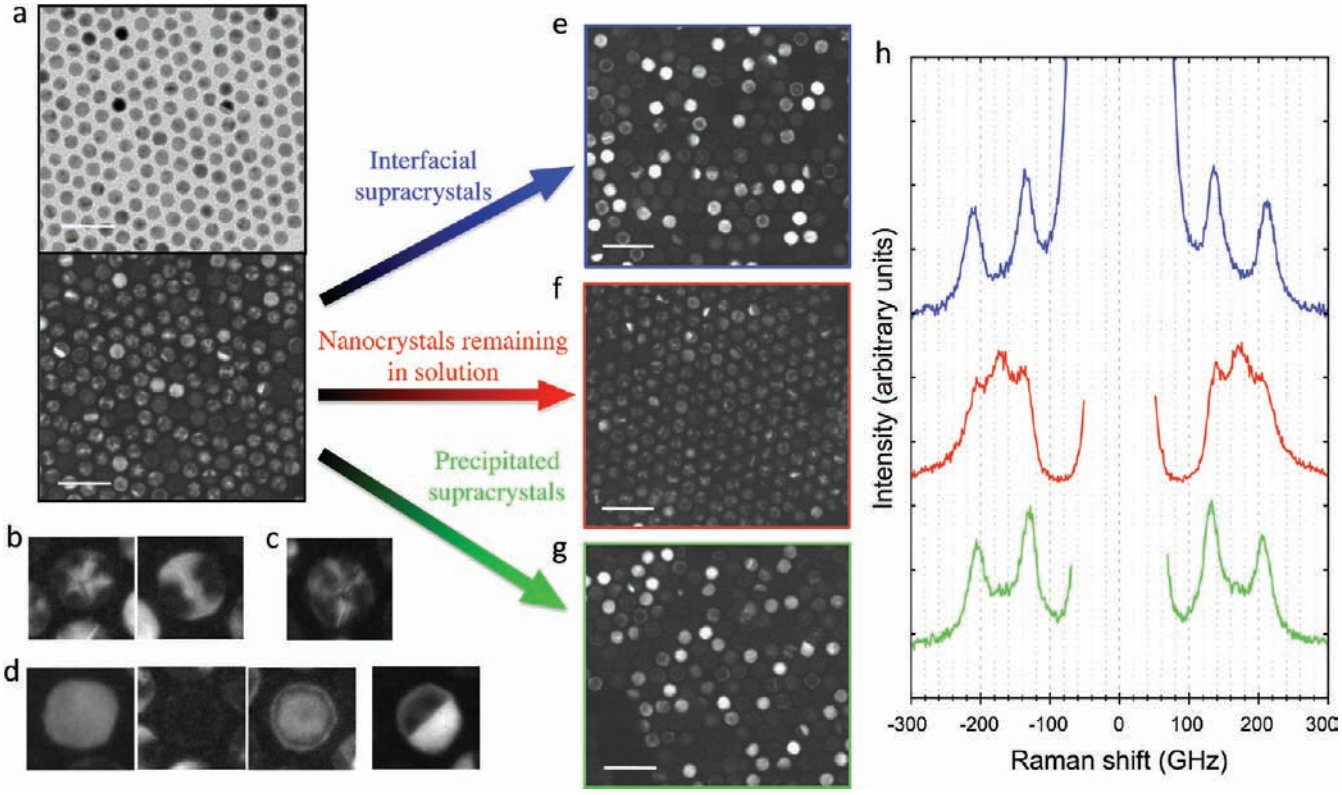

Figure 3. Bright and conical dark field images of Au_5 NCs (a). Heterogeneous contrasts corresponding to multiply twinned particles (b) and polycrystals with undefined symmetry (c). Typical contrasts observed for monocrystalline and spinel-twinned nanocrystals (d). Conical dark field images of Au_5 NCs from interfacial (e), precipitated (g) supracrystals dispersed in hexane and from the remaining colloidal solution (f), the scale bar is 20 nm. Anti-Stokes/Stokes low-frequency Raman spectra (λ_{exc}= 561 nm) of interfacial and precipitated supracrystals (blue and green curves respectively) and colloidal solution (red curve) of Au_5 NCs. The spectra are vertically shifted and independently scaled for clarity (h).

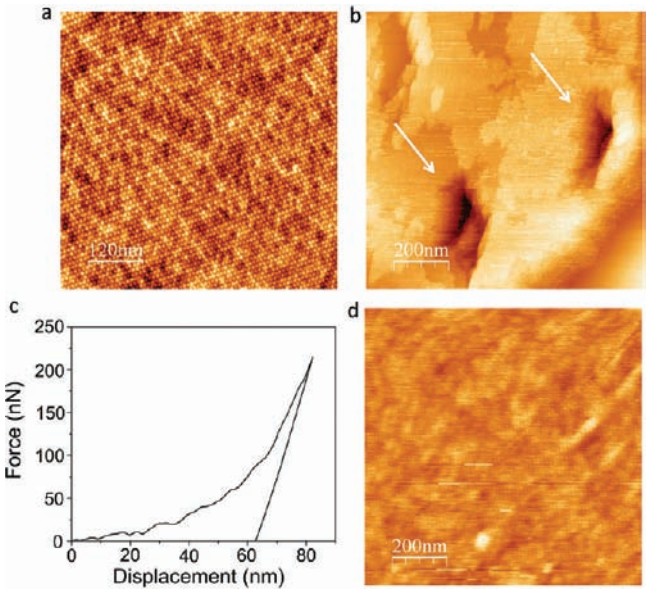

Figure 4. AFM image (600 × 600 nm^2) of interfacial Au_8 supracrystal in tapping mode (a). Indentation mark on the supracrystal surface (b). Typical load and unload versus indentation–penetration curve of gold supracrystal (c). AFM image (1 ×1 μm^2) of a precipitated supracrystal in contact mode (d).

(SC1) or MTP (SC2) nanocrystals. To provide this supracrystals, the interfacial supracrystals are dissolved in hexane, and then the solvent is evaporated with formation of SC1 layer-by-layer supracrystals. To obtain SC2 NCs, the solution remaining between the interfacial and precipitated supracrystals is extracted. At the end of toluene evaporation SC2 NCs are produced. Because the nanocrystallinity segregation is fully realized with Au_5, the SC1 and SC2 supracrystal films are both composed of Au_5. Then, the elastic moduli of SC1 and SC2 films are also measured by nanoindentation, and the SC2 film is found to be much softer than the SC1. During the experiments, a softer tip with spring constant of 0.08 N/m is used to avoid breaking the SC2 films, which was inevitable with standard 4.5 N/m tips. Results show that the elastic modulus of SC2 is almost 2 orders of magnitude smaller than that of SC1. The decrease in the Young's modulus with increasing the NC size (Table 1) is explained by a decrease in the nanocrystallinity selection with formation of supracrystals composed by mixed (single crystals–MTPs–polycrystals) population. However, such decreases could also be partly attributed to a change in the density because the average distance between nanocrystals in the supracrystals remains unchanged when the NC sizes increase. These data are different from previous ones that show an increase in the Young's modulus with increasing NC sizes for various interparticle distances.[12] These later results concerned semiconductors in which the nanocrystallinity was not taken into account. As demonstrated in the present study, the nanocrystallinity is the key parameter to produce stiff supracrystals that could be relevant for future applications.

dx.doi.org/10.1021/ja207941p | J. Am. Chem. Soc. 2012, 134, 3714–3719

4. CONCLUSION

Here we have succeeded in achieving simultaneous growths of two separate types of supracrystals from the same NC mother suspension. These growth mechanisms, at the quasi-equilibrium, permit production of highly homogeneous supracrystals with very few defects and unexpected physical properties. Hence, nanocrystallinity selection with formation of supracrystals of monodomain NCs is achieved, while MTPs and polycrystals remain in solution. This is a new route to produce a large collection of nanocrystals composed either of monodomain NCs or MTPs and polycrystals. The challenge in selectively producing monodomain NCs is achieved more easily than with the existing synthesis process. Furthermore, the nanocrystallinity is a key parameter for the production of supracrystals with Young's modulus in the GPa range. The mechanical properties of supracrystals investigated in the present study highlight dependence on both supracrystal growth mechanism and the nanocrystallinity.

■ ASSOCIATED CONTENT

Ⓢ Supporting Information

Elastic modulus determination, Raman spectrum measurements. This material is available free of charge via the Internet at http://pubs.acs.org.

■ AUTHOR INFORMATION

Corresponding Author

marie-paule.pileni@upmc.fr

Notes

The authors declare no competing financial interest.

■ ACKNOWLEDGMENTS

We thank Pr P. Kamat from University of Notre Dame, Indiana, and Dr B. Abecassis, T.Cren, J.Richardi, and P.Yang for fruitful discussions. The C.Y. research leading to these results has received funding from the European Community Seventh Framework Programme (FP7/2008-2011) under Grant Agreement no. 213382.

■ REFERENCES

(1) Nozawa, J.; Tsukamoto, K.; van Enckevort, W.; Nakamura, T.; Kimura, Y.; Miura, H.; Satoh, H.; Nagashima, K.; Konoto, M. *J. Am. Chem. Soc.* **2011**, *133*, 8782−8785.
(2) Sanders, J. V. *Nature* **1964**, *204*, 1151−1153.
(3) Motte, L.; Billoudet, F.; Pileni, M. P. *J. Phys. Chem.* **1995**, *99*, 16425−16429.
(4) Murray, C. B.; Kagan, C. R.; Bawendi, M. G. *Science* **1995**, *270*, 1335−1338.
(5) Mueggenburg, K. E.; Lin, X.-M.; Goldsmith, R. H.; Jaeger, H. M. *Nat. Mater.* **2007**, *6*, 656−660.
(6) Cheng, W.; Campolongo, M. J.; Cha, J. J.; Tan, S. J.; Umbach, C. C.; Muller, D. A.; Luo, D. *Nat. Mater.* **2009**, *8*, 519−525.
(7) Zabet-Khosousi, A.; Dhirani, A.-A. *Chem. Rev.* **2008**, *108*, 4072−4124.
(8) Klecha, E.; Ingert, D.; Pileni, M. P. *J. Phys. Chem. Lett.* **2010**, *1*, 1616−1622.
(9) Lisiecki, I.; Turner, S.; Bals, S.; Pileni, M. P.; Tendeloo, G. V. *Chem. Mater.* **2009**, *21*, 2335−2338.
(10) Milovan, U.; Bosiljka, T. *J. Phys.: Condens. Matter* **2010**, *22*, 163201.
(11) Germain, V.; Pileni, M. P. *Adv. Mater.* **2005**, *17*, 1424−1429.
(12) Podsiadlo, P.; Krylova, G.; Lee, B.; Critchley, K.; Gosztola, D. J.; Talapin, D. V.; Ashby, P. D.; Shevchenko, E. V. *J. Am. Chem. Soc.* **2010**, *132*, 8953−8960.
(13) Tanaka, A.; Kamikubo, H.; Doi, Y.; Hinatsu, Y.; Kataoka, M.; Kawai, T.; Hasegawa, Y. *Chem. Mater.* **2010**, *22*, 1776−1781.
(14) Zaitseva, N.; Dai, Z. R.; Leon, F. R.; Krol, D. *J. Am. Chem. Soc.* **2005**, *127*, 10221−10226.
(15) Pileni, M. P. *Acc. Chem. Res.* **2007**, *40*, 685−693.
(16) Nie, Z.; Petukhova, A.; Kumacheva, E. *Nat. Nano* **2010**, *5*, 15−25.
(17) Goubet, N.; Richardi, J.; Albouy, P.-A.; Pileni, M.-P. *Adv. Funct. Mater.* **2011**, *21*, 2693−2704.
(18) Dong, A.; Chen, J.; Vora, P. M.; Kikkawa, J. M.; Murray, C. B. *Nature* **2010**, *466*, 474−477.
(19) Rao, C. N. R.; Kalyanikutty, K. P. *Acc. Chem. Res.* **2008**, *41*, 489−499.
(20) Wang, S.; Sato, S.; Kimura, K. *Chem. Mater.* **2003**, *15*, 2445−2448.
(21) Talapin, D. V.; Shevchenko, E. V.; Kornowski, A.; Gaponik, N.; Haase, M.; Rogach, A. L.; Weller, H. *Adv. Mater.* **2001**, *13*, 1868−1871.
(22) Whetten, R. L.; Shafigullin, M. N.; Khoury, J. T.; Schaaff, T. G.; Vezmar, I.; Alvarez, M. M.; Wilkinson, A. *Acc. Chem. Res.* **1999**, *32*, 397−406.
(23) Harfenist, S. A.; Wang, Z. L.; Alvarez, M. M.; Vezmar, I.; Whetten, R. L. *J. Phys. Chem.* **1996**, *100*, 13904−13910.
(24) Prasad, B. L. V.; Sorensen, C. M.; Klabunde, K. J. *Chem. Soc. Rev.* **2008**, *37*, 1871−1883.
(25) Compton, O. C.; Osterloh, F. E. *J. Am. Chem. Soc.* **2007**, *129*, 7793−7798.
(26) Rupich, S. M.; Shevchenko, E. V.; Bodnarchuk, M. I.; Lee, B.; Talapin, D. V. *J. Am. Chem. Soc.* **2010**, *132*, 289−296.
(27) Courty, A.; Richardi, J.; Albouy, P.-A.; Pileni, M.-P. *Chem. Mater.* **2011**, *23*, 4186−4192.
(28) Portales, H.; Goubet, N.; Saviot, L.; Yang, P.; Sirotkin, S.; Duval, E.; Mermet, A.; Pileni, M.-P. *ACS Nano* **2010**, *4*, 3489−3497.
(29) Gu, Q. F.; Krauss, G.; Steurer, W.; Gramm, F.; Cervellino, A. *Phys. Rev. Lett.* **2008**, *100*, 045502.